Thermodynamic uncertainty theorem

Kyle J. Ray, Alexander B. Boyd, Giacomo Guarnieri, and James P. Crutchfield

Phys. Rev. E **108**, 054126 — Published 17 November 2023

DOI: 10.1103/PhysRevE.108.054126

The Thermodynamic Uncertainty Theorem

Kyle J. Ray,[1,*] Alexander B. Boyd,[2,3,4,†] Giacomo Guarnieri,[5,‡] and James P. Crutchfield[1,§]

[1] *Complexity Sciences Center and Department of Physics and Astronomy, University of California at Davis, One Shields Avenue, Davis, CA 95616, USA*
[2] *Corresponding author*
[3] *Division of Physics, Mathematics, and Astronomy, California Institute of Technology, Pasadena, CA 91125, USA*
[4] *School of Physics, Trinity College Dublin, College Green, Dublin 2, D02 PN40, Ireland*
[5] *Dahlem Center for Complex Quantum Systems, Freie Universität Berlin, 14195 Berlin, Germany*

Thermodynamic uncertainty relations (TURs) express a fundamental lower bound on the precision (inverse scaled variance) of any thermodynamic charge—e.g., work or heat—by functionals of the average entropy production. Relying on purely variational arguments, we significantly extend TUR inequalities by incorporating and analyzing the impact of higher statistical cumulants of the entropy production itself within the general framework of time-symmetrically controlled computation. We derive an exact expression for the charge that achieves the minimum scaled variance, for which the TUR bound tightens to an equality that we name *Thermodynamic Uncertainty Theorem* (TUT). Importantly, both the minimum scaled variance charge and the TUT are functionals of the stochastic entropy production, thus retaining the impact of its higher moments. In particular, our results show that, beyond the average, the entropy production distribution's higher moments have a significant effect on any charge's precision. This is made explicit via a thorough numerical analysis of "swap" and "reset" computations that quantitatively compares the TUT against previous generalized TURs.

Keywords: thermodynamic uncertainty relation, entropy production, nonequilibrium steady state, current, charge

INTRODUCTION

Recent decades witnessed substantial technological advances in miniaturization that, today, have culminated in experimental realizations of nanoscale thermal machines [1–8]. These devices exhibit three fundamental features. First, they operate under nonequilibrium conditions, either by keeping the system in a nonequilibrium steady-state by means of voltage or temperature biases or through the application of an external time-dependent control protocol. This implies that a certain amount of entropy production Σ—a proxy for the irreversible dissipation associated with nonequilibrium processes—is always generated [9]. Crucially, entropy production limits heat engine and refrigerator performance, constrains the physical mechanisms underlying complex biological functioning [10], and is the central quantity in Landauer's information erasure—the keystone in the bridge between thermodynamics and information theory. Second, due to their microscopic nature, the fluctuations of all thermodynamic quantities—heat, work, and so on—become as significant as their average values. Last, but not least, the laws of quantum mechanics have important repercussions for fluctuations that then have both thermal and quantum origins [11–14].

Since Onsager's and Kubo's pioneering discovery of the fluctuation-dissipation relation (FDR) [15–17], determining the universal properties of fluctuations in out-of-equilibrium processes, as well as their role in dissipation, has been a cornerstone of stochastic thermodynamics. In the '90s, Jarzynski and Crooks generalized the FDR through the *fluctuation relations* (FRs) [18–29]. At the microscopic scale, the FRs refine the famous Second Law of Thermodynamics $\langle \Sigma \rangle \geq 0$ by determining the full distribution of stochastic thermodynamic quantities and thus their fluctuations. That is, the FRs replaced the familiar Second law inequality with an equality. From there, the Second Law is easily derived through Jensen's inequality.

More recently, a third milestone was crossed by connecting thermodynamic fluctuations out of equilibrium to dissipation. These broad results, called *thermodynamic uncertainty relations* (TURs), were originally discovered in nonequilibrium steady-states of classical time-homogeneous Markov jump-processes satisfying local detailed balance [30, 31]. Today, though, TURs have been generalized to finite-time processes [32–34], periodically-driven systems [35–41], Markovian quantum systems undergoing Lindblad dynamics [42–46], and autonomous classical [33, 47] and quantum [47–52] systems in steady-states close to linear response.

In all these, TURs bound the fluctuations of any (time-reversal anti-symmetric stochastic) thermody-

* kylejray@gmail.com
† alecboy@gmail.com
‡ giacomo.guarnieri@fu-berlin.de
§ chaos@ucdavis.edu

namic quantity Q by a functional of the *average* entropy production $\langle\Sigma\rangle$:

$$\epsilon_Q^2 \equiv \frac{\mathrm{var}(Q)}{\langle Q\rangle^2} \geq f(\langle\Sigma\rangle) \ . \tag{1}$$

with $\langle Q\rangle$ and $\mathrm{var}(Q) = \langle Q^2\rangle - \langle Q\rangle^2$ being the average and variance of Q, respectively. In this way, the scaled variance ϵ_Q^2 can be seen as the inverse of charge Q's signal-to-noise ratio or precision. Since f is generally a monotonically-decreasing function, TURs express the trade-off that increased precision in Q inevitably comes at the cost of more dissipation. Such a no-free-lunch statement echoes that from the above-mentioned Second Law. It differs critically, however, as it includes fluctuations of many thermodynamic quantities of interest.

Our work significantly advances this line of inquiry by treating entropy production on the same footing as other thermodynamic quantities. In determining the effect of Σ's higher statistical moments on the signal-to-noise ratio of thermodynamic charges Q we refine the r.h.s. of Eq. (1)—i.e., $f(\langle\Sigma\rangle)$—replacing it with $\langle f(\Sigma)\rangle$:

$$\epsilon_Q^2 \geq g(\langle\tanh(\Sigma/2)\rangle) \ , \tag{2}$$

where $g(x) \equiv x^{-1} - 1$. With this, the bound becomes a functional of the distribution of *stochastic* entropy production Σ. And so, critically, the bound accounts for all higher moments.

Notably, these higher moments have become a focus of attention [53] since they are particularly germane to dissipation management in nanoscale devices—devices that must be designed to tolerate large and potentially destructive fluctuations. For example, entropy production variance and skewness determine the probability of experiencing a trajectory (i.e., an experimental run) that generates extreme dissipated heat flowing through the system. This, naturally, can damage or disrupt the operation of new classes of microscopic quantum hardware [54].

In both examples, we compute Eq. (2) and quantitatively compare it against several different previously derived TUR bounds. In particular, it is important to stress that the function g appearing in our Eq. (2) agrees and reduces to a recent result obtained in Ref. [41], albeit via a completely different derivation. Our approach, moreover, focuses on realizing the bound by also finding an explicit expression for the *minimum-variance charge* that saturates Eq. (2). Finding the equality condition, in turn, allows for inverting the bound—writing the entropy production as a function of the minimizing charge.

This minimum depends sensitively on the entropy production's higher-order fluctuations. In much the same way that fluctuation theorems [19, 55, 56] reframe the Second Law from an inequality to an equality, the TUT replaces the bounds set by TUR with a saturable equality. Applying the TUT to thermodynamic simulations of bit swap and reset computations, we demonstrate that charge fluctuations can depart substantially from previous bounds set by TURs.

MINIMUM SCALED VARIANCE CHARGE

Charges Q are observations of a system $\mathcal{S}$ that change sign under time reversal. Formally, a system trajectory is the sequence $\vec{s} \equiv s_0 s_{dt} \cdots s_{\tau-dt} s_\tau$, where each $s_t \in \mathcal{S}$ is the system's state at time t. The charge associated with a reversed trajectory $R(\vec{s}) \equiv s_\tau^\dagger s_{\tau-dt}^\dagger \cdots s_{dt}^\dagger s_0^\dagger$ is minus the charge of the forward trajectory:

$$Q(R(\vec{s})) = -Q(\vec{s}) \ . \tag{3}$$

Note that the time-parity operator $\dagger$ is an identity for time-even variables and multiplies by -1 for time-odd variables.

The system $\mathcal{S}$ may be influenced by an external control parameter λ_t at every time t, thereby performing a computation over the time interval $t \in (0, \tau)$. Under (i) time-symmetric control $\lambda_{\tau-t}^\dagger = \lambda_t$ and (ii) conjugation of the distribution under the operation $\Pr(s, \tau) = \Pr(s^\dagger, 0)$, the probability of a reverse trajectory is exponentially damped by the entropy production [57]:

$$\Pr(R(\vec{s}), -\Sigma) = e^{-\Sigma} \Pr(\vec{s}, \Sigma). \tag{4}$$

This is the Detailed Fluctuation Theorem (DFT) for a Time-Symmetrically Controlled Computation (TSCC). (App. A details its derivation and scope.)

This DFT [55, 56, 58] includes NESS dynamics for which the control parameter is constant $\lambda_t = \lambda_{t'}$. It can also describe, as explored here, computations that begin in equilibrium and are then allowed to relax after the application of a time-symmetric control signal. These latter symmetries are ubiquitous in computing [59].

The symmetry imposed by TSCC imbues Q's statistics with special properties in stochastic nonequilibrium systems when compared with the entropy production Σ. To address this, we derive the exact form of the charge $Q_{\min}$ that achieves minimum scaled variance for any TSCC.

Given a TSCC operating over the time interval $[0, \tau]$, described by probability distribution $\Pr(\vec{s}, \Sigma)$ over state trajectories $\vec{s}$ and entropy productions Σ, our task is to find a charge function $Q(\vec{s}) = -Q(R(\vec{s}))$ of the state trajectories $\vec{s}$ that minimizes this scaled variance.

First, we identify a special class of *entropy-conditioned charges*, expressed as functions of the entropy production, that contain a charge with the minimum scaled variance.

Entropy-Conditioned Charge

We define the entropy-conditioned charge $q(\Sigma)$ as the average charge in the system given that system dissipated entropy Σ:

$$q(\Sigma) \equiv \sum_Q Q \Pr(Q|\Sigma) \ . \tag{5}$$

If the entropy production is a function of the state trajectory, as is the case for systems satisfying local detailed balance, then we can use the entropy-conditioned charge to define a new function of the trajectories:

$$Q'(\vec{s}) \equiv q(\Sigma(\vec{s})) \ . \tag{6}$$

Q' is a well-defined charge within the system, since $Q'(R(\vec{s})) = -Q'(\vec{s})$, as shown App. B.

On the one hand, the newly defined entropy-conditioned charge has the convenient property that its average $\langle Q' \rangle \equiv \langle q \rangle$ is the same as that for the charge used to define it:

$$\begin{aligned}
\langle Q' \rangle &= \sum_\Sigma \Pr(\Sigma) q(\Sigma) \\
&= \sum_\Sigma \Pr(\Sigma) \sum_Q Q \Pr(Q|\Sigma) \\
&= \sum_{\Sigma,Q} Q \Pr(Q,\Sigma) \\
&= \sum_Q Q \Pr(Q) \\
&\equiv \langle Q \rangle \ .
\end{aligned}$$

On the other hand, the variance of the entropy-conditioned charge is not the same. When we evaluate the average square of the newly defined charge:

$$\begin{aligned}
\langle Q'^2 \rangle &= \sum_\Sigma \Pr(\Sigma) q(\Sigma)^2 \\
&= \sum_\Sigma \Pr(\Sigma) \left(\sum_Q Q \Pr(Q|\Sigma) \right)^2 \ ,
\end{aligned}$$

we can apply Jensen's inequality—$\langle Q \rangle^2 \leq \langle Q^2 \rangle$—to show that:

$$\begin{aligned}
\langle Q'^2 \rangle &\leq \sum_\Sigma \Pr(\Sigma) \left(\sum_Q Q^2 \Pr(Q|\Sigma) \right) \\
&= \sum_{Q,\Sigma} \Pr(Q,\Sigma) Q^2 \\
&= \langle Q^2 \rangle \ .
\end{aligned}$$

As a result, the entropy-conditioned charge produces scaled variance that is less than or equal to the charge used to define it:

$$\epsilon_Q^2 \geq \epsilon_{Q'}^2 \ . \tag{7}$$

Minimizing Charge

Given that any charge's scaled variance can be reduced by finding its corresponding entropy-conditioned charge, given some TSCC process $\Pr(\vec{s}, \Sigma)$, we need only find the function $q(\Sigma)$ that minimizes the scaled variance $\epsilon_q^2 = \langle q^2 \rangle / \langle q \rangle^2 - 1$. There is a single important constraint that applies to these functions: $q(-\Sigma) = -q(\Sigma)$. Thus, the optimization is constrained.

However, we can ignore this constraint by using the TSCC DFT and summing over the state trajectories of Eq. (4) to produce a familiar relation [57, 60]:

$$\Pr(-\Sigma) = e^{-\Sigma} \Pr(\Sigma) \ . \tag{8}$$

We use this to express the average q and q^2 in terms of positive entropy productions:

$$\begin{aligned}
\langle q^2 \rangle &= \sum_{\Sigma > 0} \Pr(\Sigma)(1 + e^{-\Sigma}) q(\Sigma)^2 \\
\langle q \rangle &= \sum_{\Sigma > 0} \Pr(\Sigma)(1 - e^{-\Sigma}) q(\Sigma) \ .
\end{aligned} \tag{9}$$

Thus, ϵ_q^2 can be expressed in terms of only positive entropy productions. The consequence is that $q(\Sigma)$ is *unconstrained* over positive Σ and so the minimum occurs when:

$$\begin{aligned}
\frac{\partial}{\partial q(\Sigma)} \epsilon_q^2 &= \frac{1}{\langle q \rangle^2} \left(\frac{\partial \langle q^2 \rangle}{\partial q(\Sigma)} - \frac{2 \langle q^2 \rangle}{\langle q \rangle} \frac{\partial \langle q \rangle}{\partial q(\Sigma)} \right) \\
&= 0 \ ,
\end{aligned} \tag{10}$$

for all $\Sigma > 0$. Applying the derivative with respect to the positive-entropy charge $q(\Sigma)$ to the averages shown in Eq. (9) yields:

$$\begin{aligned}
\frac{\partial \langle q \rangle}{\partial q(\Sigma)} &= (1 - e^{-\Sigma}) \Pr(\Sigma) \\
\frac{\partial \langle q^2 \rangle}{\partial q(\Sigma)} &= (1 + e^{-\Sigma}) \Pr(\Sigma) 2 q(\Sigma) \ .
\end{aligned}$$

Finally, plugging these into Eq. (9), we solve for the charge with the minimum scaled variance. This yields our primary result:

$$\boxed{q_{\min}(\Sigma) = \frac{\langle q_{\min}^2 \rangle}{\langle q_{\min} \rangle} \frac{1 - e^{-\Sigma}}{1 + e^{-\Sigma}}} \ , \tag{11}$$

which applies as long as Σ is in the support of the entropy distribution.

Note that, even though the expression for the minimal charge was derived for $\Sigma > 0$, it applies to $\Sigma \leq 0$ as well, due to the condition that a charge must satisfy $q(-\Sigma) = -q(\Sigma)$. Indeed, $q_{\min}(0) = 0$ and:

$$\begin{aligned} q_{\min}(-\Sigma) &= \frac{\langle q^2_{\min}\rangle}{\langle q_{\min}\rangle}\frac{1-e^{\Sigma}}{1+e^{\Sigma}} \\ &= \frac{\langle q^2_{\min}\rangle}{\langle q_{\min}\rangle}\frac{e^{-\Sigma}-1}{e^{-\Sigma}+1} \\ &= -q_{\min}(\Sigma) \ . \end{aligned}$$

Thus, we found the form of the charge that minimizes scaled variance. And, it depends exclusively on the process' entropy production:

$$Q_{\min}(\vec{s}) = q_{\min}(\Sigma(\vec{s})) \ .$$

This result can also be found by recognizing that the bound described in Ref. [41] is achieved when the charge is proportional to its averaging observable.

This relation can be inverted as well. If we manage to discover a maximum-precision charge $Q_{\min}(\vec{s})$ for a thermodynamic process, then the entropy production can be exactly calculated as a function of the trajectory:

$$\boxed{\Sigma(\vec{s}) = \ln \frac{\langle Q^2_{\min}\rangle + \langle Q_{\min}\rangle Q_{\min}(\vec{s})}{\langle Q^2_{\min}\rangle - \langle Q_{\min}\rangle Q_{\min}(\vec{s})}}. \tag{12}$$

This second result provides an additional method to infer not only the average entropy production, but the entire distribution of entropy productions.

Thermodynamic Bound on Scaled Variance

For simplicity, note that we can choose any real value for $k = \langle q^2_{\min}\rangle/\langle q_{\min}\rangle$, and the entropy-conditioned charge $q_{\min}(\Sigma)$ will minimize the scaled variance. Moreover:

$$\frac{1-e^{-\Sigma}}{1+e^{-\Sigma}} = \tanh(\Sigma/2) \ .$$

Thus, whatever the TSCC entropy production distribution $\Pr(\Sigma)$ may be, the charge:

$$Q_{\min}(\vec{s}) = k\tanh(\Sigma(\vec{s})/2) \ , \tag{13}$$

sets a lower bound on all other system charges:

$$\begin{aligned} \epsilon^2_Q &\geq \epsilon^2_{Q\min} \\ &= \frac{\langle \tanh(\Sigma/2)^2\rangle}{\langle \tanh(\Sigma/2)\rangle^2} - 1 \ , \end{aligned} \tag{14}$$

where the constant $k = \langle q^2\rangle/\langle q\rangle$ was factored out.

This bound on the scaled variance is *tight*, as it is realized by our newly defined $Q_{\min}(\vec{s})$. For this reason, $\epsilon^2_{Q_{\min}}$ represents the tightest possible bound on the scaled variance for TSCC processes $\Pr(\Sigma, \vec{s})$.

Once again, the TSCC DFT—$\Pr(\Sigma) = e^{\Sigma}\Pr(-\Sigma)$—allows us to simplify:

$$\begin{aligned} \langle \tanh(\Sigma/2)^2\rangle &= \sum_{\Sigma>0} \Pr(\Sigma)(1+e^{-\Sigma})\left(\frac{1-e^{-\Sigma}}{1+e^{-\Sigma}}\right)^2 \\ &= \sum_{\Sigma>0} \Pr(\Sigma)(1-e^{-\Sigma})\left(\frac{1-e^{-\Sigma}}{1+e^{-\Sigma}}\right) \\ &= \langle \tanh(\Sigma/2)\rangle. \end{aligned} \tag{15}$$

As a result, we have the simplified bound on the scaled variance in terms of the entropy production. This yields our third and final result.

Theorem 1 (Thermodynamic Uncertainty Theorem)**.** *In a TSCC, the scaled variance of any charge Q is bounded below by Q_{min}'s scaled variance:*

$$\boxed{\epsilon^2_{Qmin} = \frac{1}{\langle \tanh(\Sigma/2)\rangle} - 1}. \tag{16}$$

The thermodynamic uncertainty theorem (TUT) echoes thermodynamic uncertainty relations in that it relates the minimum variance to the entropy production. We emphasize, though, that this contrasts with TURs [57, 60–62] in that it is an *equality* rather than an inequality. Additionally, unlike TURs, which are functions of the average entropy production $\langle\Sigma\rangle$, this bound depends on an *average of a function of the entropy*. This means that higher moments of the entropy distribution appear in the bound, not just the average entropy production $\langle\Sigma\rangle$. Specifically, with $f(x) \equiv \tanh(x/2)$, we can express the bound in terms of higher moments:

$$\epsilon^2_{Q\min} = \frac{1}{f(\langle\Sigma\rangle) + \sum_{n=2}^{\infty}\frac{f^{(n)}(\langle\Sigma\rangle)}{n!}\langle(\Sigma-\langle\Sigma\rangle)^n\rangle} - 1 \ . \tag{17}$$

Since this minimum is achievable by a well-defined charge $Q_{\min}$, it sets the tightest possible bound that can be determined using all moments of the entropy production distribution.

Equation (16) agrees and coincides with Eq. (16) of

Ref. [41], which was derived through a completely different method. Namely, it was derived by means of a "Hilbert uncertainty relation" that leverages the reproducing element implied by the Riesz representation theorem for any Hilbert space equipped with an appropriate inner product. This uncertainty relation was shown to reduce to an equation of the form of Eq. (2). Our approach is complementary as it investigates how the relation stems from thermodynamics through a detailed fluctuation theorem (DFT).

While reaching the same conclusion, our method has additional merits. First, it clearly highlights its relation to other previously generalized TUR bounds, also obtained from the requirement of a DFT. Thus, it gives quantitative comparisons, as shown shortly. Second, it determines a physically realizable *minimum-variance charge* $Q_{\min}(\vec{s})$ that saturates Eq. (16). Moreover, it provides an analytic inversion though Eq. (12) that may provide a path to new entropy production estimation methods.

Finally, it is worth pointing out that Eq. (8) holds valid also in the case of systems in nonequilibrium steady-state [24]. In this case, one can define the steady-state average current $J = \lim_{t\to+\infty} Q/t$ and its diffusion coefficient $\mathrm{Var}(J) = \lim_{t\to+\infty} \mathrm{Var}(Q)/t$ [63] and arrive at a TUT for the scaled variance ϵ_J^2 analogous to Eq. (16) except for the entropy production Σ being replaced by its rate $\sigma = \lim_{t\to+\infty} \Sigma/t$. The resulting minimum variance current $j_{\min}$ can then be found to be given by:

$$j_{\min}(\sigma) = \frac{\langle j_{\min}^2 \rangle}{\langle j_{\min} \rangle} \frac{1 - e^{-\sigma}}{1 + e^{-\sigma}} \ . \tag{18}$$

This is interestingly reminiscent of the recently introduced *hyper-accurate currents* [64, 65], defined as those possessing the maximum signal-to-noise ratio. The precision of these currents can be used, therefore, to bound the precision of any other thermodynamic current. This is much in the spirit of Eq. (18). However, the form of these currents was found within classical and quantum thermoelectrics assuming coherent transport in the Landauer-Büttiker formalism. In contrast, our work derives them by imposing the TSCC symmetry Eq. (8).

COMPARISON TO PAST UNCERTAINTY RELATIONS

The burgeoning variety of uncertainty relations [30–44, 47–49] naturally begs for direct comparisons. Here, we summarize several relevant comparisons. Barato and Seifert [61] derived the first TUR, finding that precision could not be maximized without a corresponding increase in the average entropy production:

$$\epsilon_Q^2 \geq \frac{2}{\langle \Sigma \rangle} \equiv \epsilon_{\mathrm{BS}}^2 \ , \tag{19}$$

where the subscripts on the latter refer to the original Barato-Seifert (BS) bound on scaled variance.

Further exploration found that detailed fluctuation theorems [55, 56] can be used to establish modified thermodynamic uncertainty relations. Reference [57] as well as Ref. [60] used Eq. (4) to demonstrate that the scaled variance is bounded below by:

$$\epsilon_Q^2 \geq \frac{2}{e^{\langle \Sigma \rangle} - 1} \equiv \epsilon_{\mathrm{HVV}}^2 \tag{20}$$

$$\epsilon_Q^2 \geq \mathrm{csch}^2[g(\langle \Sigma \rangle/2)] \equiv \epsilon_{\mathrm{TGGL}}^2 \ , \tag{21}$$

where $g(x)$ is the inverse of $x \tanh(x)$. (We again label bounds for the authors.) The $\epsilon_{\mathrm{TGGL}}^2$ bound is the tightest possible bound on scaled variance that can be determined from the average entropy [60]. Comparing these bounds independent of the TUT, one sees in Figs. 1 and 2 that they are ordered:

$$\epsilon_{\mathrm{BS}}^2(\langle \Sigma \rangle) > \epsilon_{\mathrm{TGGL}}^2(\langle \Sigma \rangle) > \epsilon_{\mathrm{HVV}}^2(\langle \Sigma \rangle) \ . \tag{22}$$

(App. C gives a proof.) Note that, since $\epsilon_{\mathrm{TGGL}}^2$ and $\epsilon_{\mathrm{HVV}}^2$ were derived from the TSCC DFT, which is our starting point as well, the minimum scaled variance is bounded below by these TURs, but not necessarily ϵ_{BS}^2.

With $\epsilon_{Q\min}^2$'s exact form determined, though, a natural next question is how close the previous bounds, all depending only on the average entropy production $\langle \Sigma \rangle$, are to the actual minimum.

Fortunately, Ref. [60] also showed that a particular bimodal distribution:

$$\Pr_{\min}(\Sigma) \propto \delta(\Sigma - a) + e^{-a}\delta(\Sigma + a)$$

achieves the lower bound $\epsilon_{\mathrm{TGGL}}^2$. This is the simplest distribution satisfying $\Pr(-\Sigma) = e^{-\Sigma}\Pr(\Sigma)$. That is, it consists of a delta function at entropy production $\Sigma = a$ and then contains a mirror of that entropy production at $\Sigma = -a$ reduced by the exponential factor e^{-a}. Any other NESS entropy distribution can be constructed from a superposition of such distributions.

We investigate our new minimum scaled variance $\epsilon_{Q\min}^2$ by exploring a variety of possible distributions. We take a similar strategy for each, breaking the entropy distribution into the piecewise function:

$$\Pr(\Sigma|\mu,\sigma^2) = n(\mu,\sigma^2) \begin{cases} e^{\frac{(\Sigma-\mu)^2}{2\sigma^2}} & \text{if } \Sigma \geq 0 \\ e^{\Sigma} e^{\frac{(-\Sigma-\mu)^2}{2\sigma^2}} & \text{if } \Sigma < 0 \end{cases} \ . \tag{23}$$

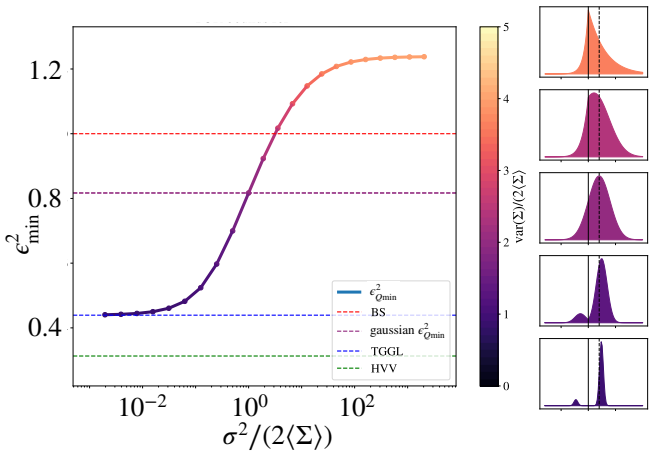

Figure 1. Thermodynamic Uncertainty Theorem versus TURs: Three dashed lines show previous TURs—$\epsilon^2_{\rm BS}$, $\epsilon^2_{\rm HVV}$, and $\epsilon^2_{\rm TGGL}$—all functions of average entropy production $\langle\Sigma\rangle$. While they make nearly identical predictions for small entropy production, they diverge as entropy increases, setting very different bounds for average entropy production as low as $\langle\Sigma\rangle = 2k_{\rm B}$. In contrast, the minimum scaled variance $\epsilon^2_{Q\min}$ is not strictly a function of average entropy. The entropy distribution $\Pr(\Sigma|\mu,\sigma^2)$ depends on the variance parameter σ^2 and is displayed on a sliding scale from high to low variance (from light to dark). σ^2 ranges from $\approx 8\times10^{-3}$ to 8×10^{3}, while μ is adjusted to keep $\langle\Sigma\rangle = 2$. This yields entropy distributions of the form shown on the right. The lowest values of Σ^2 and $\mathrm{var}(\Sigma)$ closely match $\epsilon^2_{\rm TGGL}$. As σ^2 increases, the variance of the entropy production increases and the curve becomes lighter, achieving and surpassing the dashed line for $\epsilon^2_{\rm BS}$. Between these two extremes, there is a purple dashed line that gives the minimum scaled variance of normal entropy distributions.

Here:

$$n(\mu,\sigma^2) = \int_0^\infty e^{\frac{(\Sigma-\mu)^2}{2\sigma^2}}\,d\Sigma + \int_{-\infty}^0 e^{\Sigma} e^{\frac{(-\Sigma-\mu)^2}{2\sigma^2}}\,d\Sigma$$

is the normalization factor. In essence, our probability distribution is a normal distribution with average μ and variance σ^2 over the positive interval. And, the TSCC DFT defines the distribution to be $\Pr(\Sigma) = e^{\Sigma}\Pr(-\Sigma)$ on the negative interval.

The variance σ^2 and average μ of the positive entropy portion determine the distribution $\Pr(\Sigma|\mu,\sigma^2)$. In the limit $\sigma^2 \ll k_B\mu$, the positive entropy distribution is nearly a delta function, roughly recovering the distribution $\Pr_{\min}(\Sigma)$ proposed by Ref. [60]. The left side of Fig. 1 shows this, where $\sigma^2 \approx 10^{-3}k_B\mu$, corresponding to a two-peaked distribution. In this case, $\epsilon^2_{Q\min}$ closely matches the bound $\epsilon^2_{\rm TGGL}$, as expected. However, Fig. 1 also shows that the average entropy production is not the sole determinant of the charge's minimum scaled variance.

As the variance σ^2 of the positive normal distribution increases, Fig. 1 shows that the minimum scaled variance increases. Amidst that progression is a special distribution, where $\sigma^2 = 2k_B\mu$, for which $\Pr(\Sigma|\mu,\sigma^2)$ is a normal distribution over the full range of entropy production. It can be directly shown that the variance for a normal distribution that satisfies the TSCC DFT must be $\sigma^2 = 2k_B\mu$. We highlight this special case with a purple dashed line in Fig. 1 and a blue dashed line in Fig. 2. NESS systems under Markovian dynamics, the most frequently studied subclass of TSCC processes, approach a normal entropy production distribution in the long-time limit provided they are ergodic. (See App. D.) Interestingly, the minimal variance charges of the typical asymptotic behavior in NESSs clearly violate the original TUR given by $\epsilon^2_{\rm BS}$ in the long-time limit.

If we continue beyond the normal distribution to higher variances depicted with lighter colors in Fig. 1, the minimum scaled variance $\epsilon^2_{Q\min}$ continues to increase, until it surpasses the bound $\epsilon^2_{\rm BS}$ [61]. Thus, by changing the parameter σ^2 of the NESS distribution $\Pr(\Sigma|\mu,\sigma^2)$ and its variance $\mathrm{var}(\Sigma)$ as well as other higher moments of the entropy distribution $\Pr(\Sigma)$, the TUT interpolates between the $\epsilon^2_{\rm TGGL}$ and $\epsilon^2_{\rm BS}$ TURs. Moreover, we can find entropy distributions that far exceed even the $\epsilon^2_{\rm BS}$ bound.

THERMODYNAMIC SIMULATIONS

The entropy production distribution $\Pr(\Sigma|\mu,\sigma^2)$ is convenient to examine, but it is not obvious how it can be physically generated. We now describe two computational protocols that are able to show similar breadth of behavior, but are firmly rooted in dynamical models of physical processes. Both are TSCCs in that they are implemented with time symmetric control of a potential energy landscape. The thermal influence of the environment is simulated using Langevin dynamics.

Both TSCC protocols used to generate Fig. 2 follow the same qualitative structure. The system begins in equilibrium with a thermal reservoir, exposed to a storage potential $U^{\rm store}$. At $t = 0$, a computational potential $U^{\rm comp}$ is applied until a time $t = t_1$ and then the system is re-exposed to $U^{\rm store}$ and allowed to relax back to equilibrium. The stochastic entropy production over the entire trajectory $\vec{x}$ is given by the stochastic work $w(\vec{x})$, since the free energy change is zero:

$$\beta^{-1}\Sigma(\vec{x}) = w(\vec{x}) - \Delta F \tag{24}$$
$$= w(\vec{x})\ . \tag{25}$$

Since the potential energy is fixed except for the two quenches at times $t = 0$ and $t = t_1$, the stochastic work is given by the sum of the work invested during these

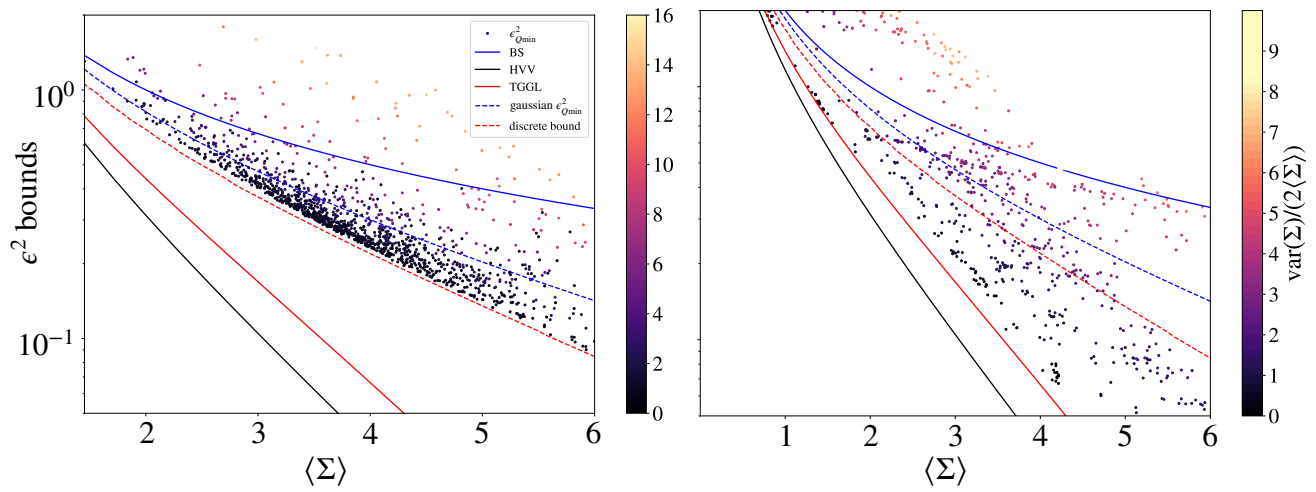

Figure 2. Comparing TURs: Bounds $\epsilon^2_{\rm BS} > \epsilon^2_{\rm TGGL} > \epsilon^2_{\rm HVV}$ in solid lines (blue, red, and black, respectively) and specific thermal processes with dashed lines. The blue dashed line is the minimum scaled variance $\epsilon^2_{\rm Gaussian}$ of any process that generates a Gaussian entropy production distribution, which is achieved in the long-time limit of NESS processes; see App. D. The red dashed line is the minimum scaled variance $\epsilon^2_{\rm Discrete}$ of an ideal discrete erasure. We compare two computational classes to the these bounds. (Left) we plot 1366 different time-symmetric erasures. As expected (see App. E 1) they are bounded by the scaled variance of the ideal discrete erasure $\epsilon^2_{\rm Discrete}$, which lies well above the bounds $\epsilon^2_{\rm TGGL}$ and $\epsilon^2_{\rm HVV}$. A number of erasure operations are well above the minimum $\epsilon^2_{\rm TGGL}$ set by $\epsilon^2_{\rm BS}$. (Right) we plot the result 1193 different bit-swaps. As with the erasure protocol, many computations are above the $\epsilon^2_{\rm BS}$ bound. However, many computations achieve a minimum scaled variance well below the discrete erasure bound $\epsilon^2_{\rm Discrete}$. Many computations are quite close to the strongest possible TUR $\epsilon^2_{\rm TGGL}$, indicating that this theoretical bound is indeed achievable with TSCCs.

quenches, w_0 and w_1. Thus, the entropy generated by a trajectory from $t = 0$ until $t = \tau_{eq}$ when the system equilibrates can be calculated from its coordinates at $t = 0$ and $t = t_1$ as:

$$\begin{aligned}\beta^{-1}\Sigma(\vec{x}) =& w_0 + w_1 \\ =& U^{\rm comp}(x_0) - U^{\rm store}(x_0) \\ &+ U^{\rm store}(x_1) - U^{\rm comp}(x_1)\ . \end{aligned} \tag{26}$$

(Note that τ_{eq} is generally longer than t_1, but need not be much longer if the system relaxes quickly) A large enough ensemble of initial conditions allows for an estimate of the entropy production distribution and, through Eq. (16), for an estimate of the minimum scaled variance that can be achieved by any charge defined on the system.

Reset

First, consider a simple reset protocol. Here, $U^{\rm store}$ is an asymmetric double square-well potential with wells of depths D_0 and D_1, widths ℓ, and centered at $x = \pm L$. (See Fig. 3.) A system x is initially set up in equilibrium with this potential at a temperature T. The $U^{\rm comp}$ for the reset is shown in Fig. 3. The left well is turned into a ramp leading to the right one, and the right well's energy is lowered. This causes nearly all realizations of the process to fall into the right well, hence the name "reset".

As the wells narrow, the variance of different work values conditioned on being in the left or right at $t = 0$ shrinks—with the intent of mirroring the narrow bimodal distribution considered in the previous section. The analysis in the preceding sections suggests that the minimum scaled variance for a narrow bimodal distribution, as calculated by Eq. (16) should agree with the $\epsilon^2_{\rm TGGL}$ bound. However, this distribution can never be a true bimodal distribution due to the necessary presence of zero entropy production events.

The presence of these events causes the true $\epsilon^2_{Q\rm min}$ to be somewhat larger than $\epsilon^2_{\rm TGGL}$. To investigate this, a suite of 1366 simulations was performed using overdamped Langevin dynamics to simulate trajectories while using a Monte Carlo Markov Chain (MCMC) inspired approach to find parameters for which $\epsilon^2_{Q\rm min}$ is minimized (See App. E 2 for simulation parameters and details.) Figure 2 shows the resulting entropy productions in minimum-variance charges. Some computations are considerably less precise than specified by $\epsilon^2_{\rm BS}$—the original TUR—but many lie well below this bound. As expected, all computations are less precise than the bounds $\epsilon^2_{\rm TGGL}$ and $\epsilon^2_{\rm HVV}$, but none of them come very close to the tightest theoretical bound given by $\epsilon^2_{\rm TGGL}$.

The result of the minimization provides numerical evi-

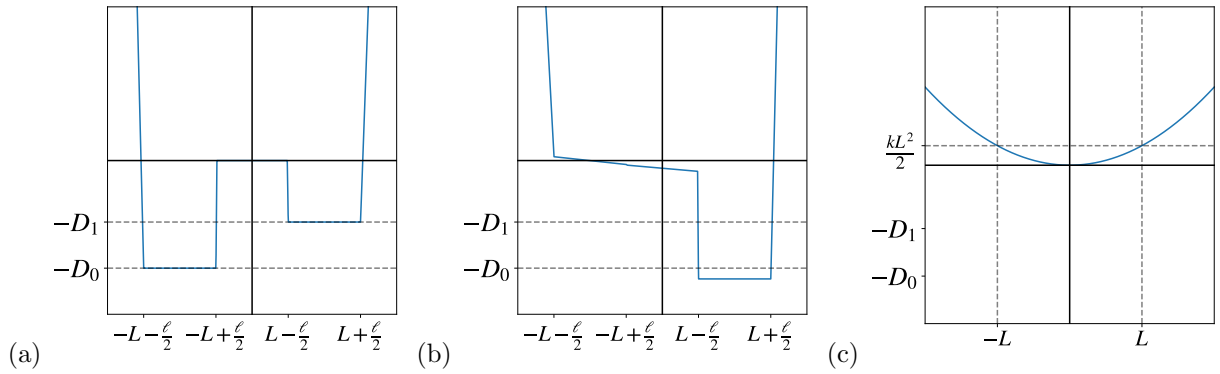

Figure 3. Potential energy landscapes during (a) storage (U^{store}), (b) the reset computation, and (c) the swap computation. The offset from D_0 in the right well during the reset computation creates the same energy barrier as the left well during the storage potential.

dence that the reset operations do indeed follow a bound above ϵ^2_{TGGL}. Further investigation revealed that the TUT can be easily specialized to a 2-level rate-equation system that, in turn, provides an analytic expression for a "discrete bound", derived in App. E 1. While this bound lies below the one for a normally distributed entropy production, Fig. 2 shows that it lies far above previous bounds—ϵ^2_{TGGL} and ϵ^2_{HVV}—that used only the TSCC DFT in Eq. (4). The reset process simulations are numerical evidence that the bound is, miraculously, quite tight for the continuous-space Langevin system despite being derived using a discrete-state system; see Fig. 2. This example showcases Eq. (16)'s flexibility, as we see it can be used to set operationally useful regime and/or protocol specific bounds by including information about the system of interest.

Swap

The swap operation has the same U^{store}, but the computational potential for the swap is a harmonic potential (see Fig. 3). If the system were isolated, it would undergo a harmonic oscillation. Exactly halfway through the oscillation, the particles that were in the left (right) well of U^{store} would be located where the right (left) well is. Thus, turning U^{store} back on at this point would implement a "swap" operation between asymmetric wells. This type of protocol also persists for underdamped dynamics: the system undergoes the same oscillation approximately, with some amount of dissipation and stochasticity. The work cost to implement this protocol approaches a bimodal distribution, with particles starting in the left well costing an energy value near $D_0 - D_1$ and those starting in the right yielding an energy surplus near $D_1 - D_0$. This distribution is sharpened by narrower wells and lower damping coefficients.

Rather than minimizing $\epsilon^2_{Q\text{min}}$, the point of this simulation is to showcase that $\epsilon^2_{Q\text{min}}$ faithfully captures all cases—from where ϵ^2_{TGGL} is tight to where ϵ^2_{BS} is tight to where neither is a good approximation. The protocol described above generates the bimodal distribution that saturates ϵ^2_{TGGL} under some cases, but can also produce entropy production distributions where the minimal scaled variance is well above ϵ^2_{BS}. To showcase this variety, a parameter-searching algorithm was used to explore the space of $\epsilon^2_{Q\text{min}}$ over 1193 parameter sets rather than the minimization algorithm in the reset simulations. Again, the simulation details and parameters can be found in App. E 3. The entropy and scaled variance of these swaps are shown on the right-hand side of Fig. 2. They span the same space of possibilities shown for $\Pr(\Sigma|\mu,\sigma^2)$ in Fig. 1: some lying above ϵ^2_{BS} and some TSCCs sitting just above the minimum set by ϵ^2_{TGGL}.

For both the reset and swap, we see that the minimum scaled variance tends to increase as the variance of the entropy-production distribution increases. In short, higher moments of entropy production are critically important in predicting the precision of computations.

CONCLUSION

We introduced two equalities that provide an explicit expression for the most accurate charge in any entropy production distribution that satisfies Eq. (4) and for the minimal scaled variance it achieves. Analogous to the transition from the Second Law inequality to the fluctuation relations of Crooks and Jarzynski, we developed a treatment of the entropy production that recognizes it as a stochastic quantity with proper fluctuations. This treatment yields a result—the Thermodynamic Uncertainty Theorem—that (i) is an equality rather than an inequality and (ii) depends on the stochastic entropy pro-

duction's fluctuations rather than on only its average value.

Equation (12) provides an inversion of the TUT—an expression for the entropy production as a function of the minimizing charge Q_{min}. Methods for estimating entropy production using TUR saturation conditions have already been established and tested [66–69] and so a natural continuation of this is to apply these methods to TUT inversion as well. The previous analyses have been limited to short-time behavior, systems that saturate the ϵ^2_{BS} bound or to systems obeying Langevin dynamics. Analogous investigations of the TUT, being derived under very general assumptions, may provide an important missing piece to these previous explorations.

The TUT also allows for straightforward derivations of new system- or dynamic-specific TURs. Our simulations demonstrated that overdamped reset operations adhere to their TUT-derived bound $\epsilon^2_{\mathrm{Discrete}}$, while the underdamped swap operations are free of $\epsilon^2_{\mathrm{Discrete}}$ and can approach the $\epsilon^2_{\mathrm{TGGL}}$ bound. Tuning the higher moments of entropy production allows us to interpolate between the maximum precision $\epsilon^2_{\mathrm{TGGL}}$ set by Ref. [60] and the original TUR $\epsilon^2_{\mathrm{BS}} = 2/\langle\Sigma\rangle$ [61]. Nonequilibrium steady states generally approach a Gaussian entropy-production distribution, so their higher moments produce charges that are more precise than predicted by ϵ^2_{BS} but less precise than $\epsilon^2_{\mathrm{TGGL}}$.

Our simulations showed that there are both reset and swap operations for which the minimum variance charge is even less precise than predicted by ϵ^2_{BS}. The relationship indicates that, independent of the average entropy production, higher variance in the entropy production leads to less precise charges. This analysis opens up the opportunity to investigate, in more detail, the specific effects that higher moments impose upon the entropy production. Equation (17) gives the formal relationship, but it remains to be seen how these effects manifest in practice.

Acknowledgements We thank John Goold and Felix Binder for helpful discussions and Gianmaria Falasco, Massimiliano Esposito, and Jean-Charles Delvenne for alerting us to Ref. [41]. The authors thank the Telluride Science Research Center for hospitality during visits and the participants of the Information Engines Workshops there. A.B.B. acknowledges support from the Templeton World Charity Foundation Power of Information fellowships TWCF0337 and TWCF0560 and from the Foundational Questions Institute and Fetzer Franklin Fund, a donor advised fund of the Silicon Valley Community Foundation, grant number FQXi-RFP-IPW-1910. J.P.C. and K.J.R. acknowledge support by, or in part by, U.S. Army Research Laboratory and the U.S. Army Research Office under grant W911NF-18-1-0028. G.G. acknowledges support from Foundational Questions Institute and DFG FOR2724 and also from the European Union Horizon 2020 Research and Innovation Programme under Marie Sklodowska-Curie grant agreement No. 101026667.

Appendix A: Time Symmetrically Controlled Computation Detailed Fluctuation Theorem

While Crooks originally derived the Detailed Fluctuation Theorem (DFT) within the context of detailed balanced Markov dynamics [56], Jarzynski provided an elegant proof of a generalization with a rather appealing set-up [55]. With a system $\mathcal{S}$ that is controlled by an external parameter and weakly coupled to a collection of thermal reservoirs (each specified by its respective temperature T), he proved that the joint probability of a state trajectory $\vec{s} \equiv s_0 s_{t_1} \cdots s_{t_{N-2}} s_\tau$ and the environmental entropy production, defined as the heat entropy generated in each reservoir:

$$\mathcal{Q} \equiv \sum_T \frac{\mathcal{Q}_T}{T},$$

is exponentially damped under time reversal. This framework can be applied to a wide variety of computations over the time interval $t \in (0, \tau)$ and can operate without the constraints of detailed balance, since there are multiple reservoirs.

Specifically, using random variable notation where capital letters denote the random variable and lower case letters denote their realizations, Ref. [55] shows that:

$$\frac{\Pr(\mathcal{Q} = -\mathbf{q}, \vec{S} = R(\vec{s}) | S_0 = s_\tau^\dagger, \vec{\Lambda} = R(\vec{\lambda}))}{\Pr(\mathcal{Q} = \mathbf{q}, \vec{S} = \vec{s} | S_0 = s_0, \vec{\Lambda} = \vec{\lambda})} = e^{-\mathbf{q}}, \quad \text{(A1)}$$

where we set Boltzmann's constant to $k_B = 1$ for ease of notation. Here, control protocol $\vec{\lambda} \equiv \lambda_0 \cdots \lambda_\tau$ is the parameter trajectory over the computation interval $(0, \tau)$. The time reversal operator R operates on trajectories by reversing the sequence and flipping the sign of time-antisymmetric variables (e.g., magnetic fields and momentum): $R(\vec{\lambda}) \equiv \lambda_\tau^\dagger \cdots \lambda_0^\dagger$. Beyond weak coupling, Ref. [55] assumes Hamiltonian dynamics and that the thermal baths are initially independently distributed in their respective Boltzmann distributions.

This differs from the Crooks fluctuation theorem in that $\vec{s}$ represents a potentially discrete sequence of states taken at potentially irregular times $t_i \in (0, \tau)$ and in that it also includes dependence on the entropy production $\mathcal{Q}$ in the probability. However, in the limit (i) where $\vec{s}$ constitutes a nearly complete description of the state trajectory, (ii) the environmental entropy production is

a deterministic function of the state trajectory, and (iii) there is only one heat bath, the results of Refs. [55, 56] are similar.

In essence, both detailed fluctuation theorems recover thermodynamic properties of a forward experiment by comparing trajectory probabilities to those of a reverse experiment. The forward experiment is determined by the control protocol $\vec{\lambda}$, which determines the probability of state trajectories and heats conditioned on the initial state S_0, but also depends sensitively on the initial distribution of the system $f_0(s_0)$. f is used to indicate that it is the probability of the forward experiment, and the subscript 0 indicates initial time $t = 0$. This then provides the instantaneous distribution of the system in the forward experiment at all times t:

$$f_t(s) \equiv \sum_{s_0} \Pr(S_t = s | S_0 = s_0, \vec{\Lambda} = \vec{\lambda}) f_0(s_0) \ .$$

Similarly, the reverse experiment must be prepared in some distribution $r_0(s_0)$, yielding the instantaneous distribution of the system in the reverse experiment at all times:

$$r_t(s) \equiv \sum_{s_0} \Pr(S_t = s | S_0 = s_0, \vec{\Lambda} = R(\vec{\lambda})) r_0(s_0) \ .$$

The state of preparation of the forward and reverse experiment is essential for determining the system's total entropy production.

The total entropy production due to control $\vec{\lambda}$ in the forward experiment must also include the change in system surprisal [70]:

$$\Sigma = \mathbf{q} + \ln \frac{f_0(s_0)}{f_\tau(s_\tau)} \ .$$

Substituting into the DFT of Eq. (A1), yields a relation for total entropy production as well:

$$\frac{\Pr(\mathcal{Q} = -\mathbf{q}, \vec{S} = R(\vec{s}) | S_0 = s_\tau^\dagger, \vec{\Lambda} = R(\vec{\lambda}))}{\Pr(\mathcal{Q} = \mathbf{q}, \vec{S} = \vec{s} | S_0 = s_0, \vec{\Lambda} = \vec{\lambda})} = e^{-\Sigma + \ln \frac{f_0(s_0)}{f_\tau(s_\tau)}}$$

or:

$$\frac{\Pr(\mathcal{Q} = -\mathbf{q}, \vec{S} = R(\vec{s}) | S_0 = s_\tau^\dagger, \vec{\Lambda} = R(\vec{\lambda}))}{\Pr(\mathcal{Q} = \mathbf{q}, \vec{S} = \vec{s} | S_0 = s_0, \vec{\Lambda} = \vec{\lambda})} \frac{f_\tau(s_\tau)}{f_0(s_0)} = e^{-\Sigma} \ .$$

To parallel Crooks' original examination of fluctuation theorems [56], we would like to express probabilities of *total* entropy production, rather than *environmental* entropy production. En route, note that the conditional probability of total entropy production under forward control can be expressed:

$$\Pr(\Delta S_{\text{tot}} = \Sigma | \mathcal{Q} = \mathbf{q}, \vec{S} = \vec{s}, \vec{\Lambda} = \vec{\lambda}) = \delta_{\Sigma, \mathbf{q} + \ln \frac{f_0(s_0)}{f_\tau(s_\tau)}} \ .$$

We can then evaluate:

$$\Pr(\Delta S_{\text{tot}} = \Sigma, \vec{S} = \vec{s} | S_0 = s_0, \vec{\Lambda} = \vec{\lambda}) f_0(s_0) = \sum_{\mathbf{q}} \delta_{\Sigma, \mathbf{q} + \ln \frac{f_0(s_0)}{f_\tau(s_\tau,)}} \Pr(\mathcal{Q} = \mathbf{q}, \vec{S} = \vec{s} | S_0 = s_0, \vec{\Lambda} = \vec{\lambda}) f_0(s_0) \tag{A2}$$

$$\Pr(\Delta S_{\text{tot}} = \Sigma, \vec{S} = \vec{s} | \vec{\Lambda} = \vec{\lambda}) = e^{\Sigma} \sum_{\mathbf{q}} \delta_{-\Sigma, -\mathbf{q} + \ln \frac{f_\tau(s_\tau)}{f_0(s_0)}} \Pr(\mathcal{Q} = -\mathbf{q}, \vec{S} = R(\vec{s}) | S_0 = s_\tau^\dagger, \vec{\Lambda} = R(\vec{\lambda})) f_\tau(s_\tau),$$

$$\Pr(\Delta S_{\text{tot}} = \Sigma, \vec{S} = \vec{s} | \vec{\Lambda} = \vec{\lambda}) = e^{\Sigma} \sum_{\mathbf{q}} \delta_{-\Sigma, -\mathbf{q} + \ln \frac{f_\tau(s_\tau)}{f_0(s_0)}} \Pr(\mathcal{Q} = -\mathbf{q}, \vec{S} = R(\vec{s}) | \vec{\Lambda} = R(\vec{\lambda})) \ ,$$

where we introduced the unconditioned process that comes from forward control $\vec{\lambda}$ and starting in the initial distribution $f_0(s_0)$:

$$\Pr(\Delta S_{\text{tot}} = \Sigma, \vec{S} = \vec{s} | \vec{\Lambda} = \vec{\lambda}) \equiv \Pr(\Delta S_{\text{tot}} = \Sigma, \vec{S} = \vec{s} | S_0 = s_0, \vec{\Lambda} = \vec{\lambda}) f_0(s_0) \ .$$

We also introduced unconditioned process of the reverse

experiment that comes from initializing the system in the conjugate of the final distribution of the forward experiment $r_0(s) = f_\tau(s^\dagger)$ and reversing the control sequence:

$$\begin{aligned}\Pr(\mathcal{Q} = \mathbf{q}, \vec{S} = \vec{s}|\vec{\Lambda} = R(\vec{\lambda})) \\ \equiv \Pr(\mathcal{Q} = \mathbf{q}, \vec{S} = \vec{s}|S_0 = s_0, \vec{\Lambda} = R(\vec{\lambda}))r_0(s_0) \ .\end{aligned}$$

Substituting in $-\mathbf{q}$ for the environmental entropy production and $R(\vec{s})$ for the state sequence yields the right-hand term in the last line of Eq. (A2).

We want to evaluate the probability of entropy production in the reverse experiment as well. Denoting the final system distribution that results from the reverse experiment as $r_\tau(s)$, the total entropy production is:

$$\Sigma = \mathbf{q} + \ln \frac{r_0(s_0)}{r_\tau(s_\tau)} \ ,$$

meaning that:

$$\begin{aligned}\Pr(\Delta S_{\text{tot}} = \Sigma, \vec{S} = \vec{s}|\vec{\Lambda} = R(\vec{\lambda})) \\ = \sum_{\mathbf{q}} \delta_{\Sigma, \mathbf{q} + \ln \frac{r_0(s_0)}{r_\tau(s_\tau)}} \Pr(\mathcal{Q} = \mathbf{q}, \vec{S} = \vec{s}|\vec{\Lambda} = R(\vec{\lambda})) \ .\end{aligned}$$

Comparing with Eq. (A2), we evaluate the probability of realizing the reverse sequence $R(\vec{s})$ and minus the entropy production $-\Sigma$, while summing over $-\mathbf{q}$ rather than $\mathbf{q}$:

$$\begin{aligned}\Pr(\Delta S_{\text{tot}} = -\Sigma, \vec{S} = R(\vec{s})|\vec{\Lambda} = R(\vec{\lambda})) \\ = \sum_{\mathbf{q}} \delta_{-\Sigma, -\mathbf{q} + \ln \frac{r_0(s_\tau^\dagger)}{r_\tau(s_0^\dagger)}} \Pr(\mathcal{Q} = -\mathbf{q}, \vec{S} = R(\vec{s})|\vec{\Lambda} = R(\vec{\lambda})).\end{aligned}$$

If we want to satisfy a parallel equality to the Crooks fluctuation theorem:

$$\begin{aligned}\Pr(\Delta S_{\text{tot}} = \Sigma, \vec{S} = \vec{s}|\vec{\Lambda} = \vec{\lambda}) \\ = e^{\Sigma} \Pr(\Delta S_{\text{tot}} = -\Sigma, \vec{S} = R(\vec{s})|\vec{\Lambda} = R(\vec{\lambda})),\end{aligned} \tag{A3}$$

for all reverse distributions $\Pr(\mathcal{Q} = \mathbf{q}, \vec{S} = \vec{s}|\vec{\Lambda} = R(\vec{\lambda}))$, then it must be true that:

$$\delta_{-\Sigma, -\mathbf{q} + \ln \frac{f_\tau(s_\tau)}{f_0(s_0)}} = \delta_{-\Sigma, -\mathbf{q} + \ln \frac{r_0(s_\tau^\dagger)}{r_\tau(s_0^\dagger)}} \ .$$

Thus, the following must also hold:

$$\frac{f_\tau(s_\tau)}{f_0(s_0)} = \frac{r_0(s_\tau^\dagger)}{r_\tau(s_0^\dagger)} \ .$$

Since we chose $r_0(s) = f_\tau(s^\dagger)$, the final distribution of the system in the reverse experiment must be the same as the conjugate of the initial distribution in the forward experiment:

$$r_\tau(s) = f_0(s^\dagger) \ . \tag{A4}$$

This nuance was recognized in Crooks' original result [56], though it has sometimes been lost to history.

There is a litany of different cases in which $r_\tau(s) = f_0(s^\dagger)$ is violated. That is, the extension of Crooks' fluctuation theorem shown in Eq. (A3) does not hold necessarily. For instance, if we choose a control protocol that erases a uniform distribution over $\{\uparrow, \downarrow\}$, taking $f_0(s) = 1/2$ to $f_\tau(s) = \delta_{s,\downarrow}$, but does so time symmetrically, then $r_\tau(s) = \delta_{s,\downarrow} \neq f(s^\dagger) = 1/2$.

However, in the special case of time-symmetric control—$R(\vec{\lambda}) = \vec{\lambda}$—we see a useful simplification. If the final distribution of the forward experiment happens to conjugate the initial state distribution—$f_\tau(s) = f_0(s^\dagger)$—then the initial distribution of the reverse control experiment is the same for the forward control—$r_0(s) = f_0(s)$. The resulting final system distribution under reverse control is also the same—$r_\tau(s) = f_\tau(s)$—since the forward and reverse experiment apply the same control protocol to the same initial distribution.

This guarantees the condition in Eq. (A4) that $r_\tau(s) = f_0(s^\dagger)$. And so, we see that:

$$\Pr(\Sigma, \vec{s}) = e^{\Sigma} \Pr(-\Sigma, R(\vec{s})) \ ,$$

where we shortened the notation to $\Pr(\Sigma, \vec{s}) \equiv \Pr(\Delta S_{\text{tot}} = \Sigma, \vec{S} = \vec{s}|\vec{\Lambda} = \vec{\lambda})$ for convenience. This is the *Time-Symmetric Control Computation Detailed Fluctuation Theorem* (TSCC DFT) that follows from assuming time-symmetric control $\vec{\lambda} = R(\vec{\lambda})$ and conjugating the state distribution under the computation $f_\tau(s) = f_0(s^\dagger)$.

This differs slightly but importantly from the conditions for the TSCC DFT described in Ref. [57] that instead assumed the starting state is preserved—$f_\tau(s) = f_0(s)$—under the computation. This assumption may fail to produce the desired fluctuation theorem if the control acts differently on the conjugate of the initial distribution. In this case, the computation has a different effect on the starting distribution of the reverse protocol $r_0(s) \equiv f_\tau(s^\dagger)$, which is also equal to the conjugate of the initial distribution of the forward experiment, since $f_\tau(s^\dagger) = f_0(s^\dagger)$. The distribution will not be preserved under the computation: $r_\tau(s) \neq r_0(s)$. Since $r_0(s) = f_0(s^\dagger)$, the condition for the DFT in Eq. A4 is not met. The assumptions of Ref. [57] are sufficient, though, when the initial distribution is time reversal symmetric—$f_0(s^\dagger) = f_0(s)$. The latter is often the case in biochemical systems, where the time-antisymmetric momentum variables are thermalized with respect to a single heat bath. This is also the case for many NESSs.

Appendix B: Well-defined charge

Let us define a function Q' of state trajectories in terms of the entropy-conditioned charge:

$$Q'(\vec{s}) \equiv q(\Sigma(\vec{s})) \ ,$$

where the entropy conditioned charge is defined:

$$q(\Sigma) \equiv \sum_Q Q \Pr(Q|\Sigma) \ .$$

Note that we can evaluate Q' for the time-reversal of a trajectory:

$$Q'(R(\vec{s})) = q(\Sigma(R(\vec{s}))) \ .$$

The TSCC fluctuation theorem:

$$\Pr(R(\vec{s}), -\Sigma) = e^{-\Sigma} \Pr(\vec{s}, \Sigma),$$

implies both a marginalized version:

$$\Pr(-\Sigma) = e^{-\Sigma} \Pr(\Sigma) \ ,$$

as well as equality of the conditional probabilities:

$$\Pr(R(\vec{s})| - \Sigma) = \Pr(\vec{s}|\Sigma) \ .$$

Thus, the entropy conditioned charge is an odd function of the entropy:

$$\begin{aligned}
q(-\Sigma) &= \sum_Q Q \Pr(Q| - \Sigma) \\
&= \sum_{Q,\vec{s}} Q \Pr(Q, \vec{s}| - \Sigma) \\
&= \sum_{Q,\vec{s}} Q \delta_{Q,Q(\vec{s})} \Pr(\vec{s}| - \Sigma) \\
&= \sum_{\vec{s}} Q(\vec{s}) \Pr(\vec{s}| - \Sigma) \\
&= \sum_{\vec{s}} Q(R(\vec{s})) \Pr(R(\vec{s})| - \Sigma) \\
&= \sum_{\vec{s}} -Q(\vec{s}) \Pr(\vec{s}|\Sigma) \\
&= -q(\Sigma) \ .
\end{aligned}$$

Having assumed that Σ is a function of the state trajectory, we can re-express the TSSC fluctuation theorem:

$$\Pr(R(\vec{s}))\delta_{\Sigma(R(\vec{s})),-\Sigma'} = e^{-\Sigma'} \Pr(\vec{s})\delta_{\Sigma',\Sigma(\vec{s})},$$

This can only be true if the entropy production is itself a charge $\Sigma(R(\vec{s})) = -\Sigma(\vec{s})$. Thus, we see that our new function of the trajectories Q' is indeed a charge as well:

$$\begin{aligned}
Q'(R(\vec{s})) &= q(\Sigma(R(\vec{s}))) \\
&= q(-\Sigma(\vec{s})) \\
&= -q(\Sigma(\vec{s})) \\
&= -Q'(\vec{s}) \ .
\end{aligned}$$

Appendix C: Proof of $\epsilon_Q^2 \geq \epsilon_{Q\mathbf{min}}^2 \geq \epsilon_{\mathbf{TGGL}}^2$

Start by considering the expressions for the two TUR bounds $\epsilon_{q_{min}}^2$ and ϵ_{TGGL}^2. These bound the noise-to-signal ratio (or scaled variance) $\epsilon_Q^2 \equiv \mathrm{Var}(Q)/\langle Q \rangle^2$ of any charge Q—assumed to be anti-symmetric under time-reversal—in the steady-state regime under the constraint that the probability distribution for the entropy production Σ satisfies the fluctuation relation symmetry:

$$\Pr(-\Sigma) = \Pr(\Sigma) e^{-\Sigma} \ . \tag{C1}$$

Our main result is that, under no additional assumptions about the distribution over Σ, the following bound holds:

$$\begin{aligned}
\epsilon_Q^2 &\geq \epsilon_{q_{min}}^2 \\
&\equiv \frac{1}{\langle \tanh(\Sigma/2) \rangle} - 1 \ .
\end{aligned} \tag{C2}$$

Rather, the other bound, proven in Ref. [60], shows that if in addition to the above the entropy production averages and generic charge, i.e., $\langle \Sigma \rangle$ and $\langle Q \rangle$, Σ and Q are fixed and satisfy *a joint* fluctuation relation symmetry of the form:

$$\Pr(-\Sigma, Q) = \Pr(\Sigma, Q) e^{-\Sigma} \ ,$$

then the following TUR bound can be derived:

$$\begin{aligned}
\epsilon_Q^2 &\geq \epsilon_{TGGL}^2 \\
&\equiv \mathrm{csch}^2(g(\langle \Sigma \rangle/2)) \ ,
\end{aligned} \tag{C3}$$

where $g(\langle \Sigma \rangle)$ is the function inverse of $\langle \Sigma \rangle \tanh(\langle \Sigma \rangle)$.

Is there a relationship between these two bounds? The following provides an affirmative answer.

The first step re-expresses the righthand side of Eq. (C3) as:

$$\epsilon_Q^2 \geq \epsilon_{TGGL}^2 \equiv \frac{1}{\tanh^2(g(\langle \Sigma \rangle/2))} - 1$$

by using the identity $\mathrm{csch}^2(x) + 1 = 1/\tanh^2(x)$. To

proceed, define the following quantities:

$$z(\Sigma) \equiv \tanh^2\left(\frac{\Sigma}{2}\right)$$
$$h(\Sigma) \equiv \Sigma \tanh\left(\frac{\Sigma}{2}\right) \ .$$

Furthermore, introduce the inverse function of $h(\Sigma)$ and denote it g: $g(h(\Sigma)) = \Sigma$. Notice that this is possible since $h(\Sigma)$ is a monotonically increasing function of Σ whenever $\Sigma \geq 0$. This is not a limitation, since, thanks to the fluctuation relation symmetry Eq. (C1), it amounts to considering:

$$\begin{aligned}\langle(\ldots)\rangle &\equiv \sum_{\Sigma}(\ldots)\Pr(\Sigma) \\ &= \sum_{\Sigma>0}(\ldots)\Pr(\Sigma)\left(1+e^{-\Sigma}\right) \ .\end{aligned}$$

To employ these quantities note that the composite function $w(h) \equiv f(g(h))$ is a concave function of h (when $h \geq 0$), since $w'(h) > 0$ and $w''(h) < 0$. This allows exploiting Jensen's inequality where the "norm" is given by the average $\langle\ldots\rangle$ calculated with the probability distribution $\Pr(\Sigma)(1+e^{-\Sigma})$, as just noted. This gives rise to the inequality:

$$\begin{aligned}\left\langle \tanh\left(\frac{\Sigma}{2}\right)^2 \right\rangle &= \langle z(\Sigma)\rangle \\ &= \langle z(g(h(\Sigma)))\rangle \\ &\leq z(g(\langle h(\Sigma)\rangle)) \\ &= z(g(\langle\Sigma\rangle)) \ , \end{aligned} \tag{C4}$$

where the last line used the fact that $\langle\Sigma\rangle = \langle h(\Sigma)\rangle$. Notice that the quantity appearing on the the inequality's righthand side—$z(g(\langle\Sigma\rangle))$—is nothing other than the denominator in the first term of Eq. (C3)'s righthand side.

The final step to conclude the proof then consists in realizing that Eq. (15) means that inequality Eq. (C4)'s lefthand side is the denominator in the first term of Eq. (C2)'s righthand side.

In view of Eq. (C4) it immediately follows that:

$$\epsilon^2_{q_{min}} \geq \epsilon^2_{TGGL} \ .$$

Appendix D: Central Limit Theorem For Entropy Production in Markovian NESSs

A NESS's dynamics are described by a bi-infinite process $\Pr(S_{-\infty:\infty})$ that is stationary ($\Pr(S_{\tau:\tau'} = s_{\tau:\tau'}) = \Pr(S_{\tau+\Delta t:\tau'+\Delta t} = s_{\tau:\tau'})$ for all Δt. Here, $S_{\tau:\tau'} \equiv S_\tau S_{\tau+dt}\cdots S_{\tau'-dt}S_{\tau'}$. We shift trajectory notation from $\vec{s}$ to $s_{\tau:\tau'}$, since we partition the trajectory into segments $s_{\tau:\tau'}$ when establishing the central-limit theorem for entropy production.

A common assumption is that processes are Markovian [56]. In this case, a process can be expressed as the product:

$$\Pr(S_{\tau:\tau'} = s_{\tau:\tau'}) = \pi(s_\tau)\prod_{t=\tau}^{\tau'-dt} M_{s_t\to s_{t+dt}} \ ,$$

where $M_{s\to s'} \equiv \Pr(S_{t+dt} = s'|S_t = s)$ is the conditional probability of transitions between states and $\pi(s) \equiv \Pr(S_t = s)$ is the steady state probability.

Applying Crooks fluctuation theorem [56] to a NESS with fixed control, the entropy production is:

$$\begin{aligned}\Sigma(s_{\tau:\tau'})/k_B &= \ln\frac{\Pr(S_{\tau:\tau'} = s_{\tau:\tau'})}{\Pr(S_{\tau:\tau'} = R(s_{\tau:\tau'}))} \\ &= \ln\frac{\pi(s_\tau)\prod_{t=\tau}^{\tau'-dt} M_{s_t\to s_{t+dt}}}{\pi(s_{\tau'})\prod_{t=\tau}^{\tau'-dt} M_{s^\dagger_{t+dt}\to s^\dagger_t}} \ .\end{aligned}$$

Adding $\ln\frac{\prod_{t=\tau+dt}^{\tau'-dt}\pi(s_t)}{\prod_{t=\tau+dt}^{\tau'-dt}\pi(s_t)} = 0$ gives:

$$\begin{aligned}\Sigma(s_{\tau:\tau'})/k_B &= \ln\frac{\prod_{t=\tau}^{\tau'-dt}\pi(s_t)M_{s_t\to s_{t+dt}}}{\prod_{t=\tau}^{\tau'-dt}\pi(s_{t+dt})M_{s^\dagger_{t+dt}\to s^\dagger_t}} \\ &= \sum_{t=\tau}^{\tau'-dt}\ln\frac{\pi(s_t)M_{s_t\to s_{t+dt}}}{\pi(s_{t+dt})M_{s^\dagger_{t+dt}\to s^\dagger_t}} \\ &= \sum_{t=\tau}^{\tau'-dt}\Sigma(s_{t:t+dt})/k_{\mathrm{B}} \ .\end{aligned}$$

We can now appeal to the central limit theorem for Markov Chains [71].

Define a new process $\Pr(Y_{-\infty:\infty})$ that constitutes a two-time sliding window of the states $Y_t = S_tS_{t+dt}$. Since the underlying process $\Pr(S_{-\infty:\infty})$ is Markov, so is the sliding window process $\Pr(Y_{-\infty:\infty})$:

$$\begin{aligned}\Pr(Y_t = s_ts_{t+dt}|Y_{t-dt} = s_{t-dt}s_t) &\\ = \Pr(S_{t+dt} = s_{t+dt}|S_t = s_t) &\\ = M_{s_t\to s_{t+dt}} \ .&\end{aligned}$$

Also define a function of every realization of the sliding window process as the entropy production of that state sequence:

$$g(Y_t = s_ts_{t+dt}) \equiv \Sigma(s_ts_{t+dt}) \ .$$

According to the Markov Chain Central Limit Theorem, if $\Pr(Y_{-\infty:\infty})$ is ergodic, then the entropy production

over a time interval $(0, \tau)$ averaged over time τ:

$$\begin{aligned}\frac{\Sigma(S_{0:\tau})}{\tau} &= \sum_{t=0}^{\tau-dt} \frac{\Sigma(S_t S_{t+dt})}{\tau} \\ &= \sum_{t=0}^{\tau-dt} \frac{g(Y_t)}{\tau} \ ,\end{aligned}$$

approaches a normal distribution as τ becomes large. (Full conditions are described in Theorem 9 of Ref. [71].)

Note that it may be possible to generalize this to non-Markovian NESS processes by instead defining a process where individual elements are longer sliding windows $Y_t \equiv S_{t:t+\Delta t}$, and then identifying the conditions under which the total entropy splits into a sum of entropy productions over each window. However, we leave this for later exploration.

Appendix E: Simulations

The following provides details on the reset and swap simulations.

1. Discrete Bound

To see why the reset operation as described cannot generate a truly bimodal distribution, consider a simplified version of the continuous-state dynamics that implement the reset operation: a two-level system operating in the regime of rate equation dynamics.

Here, the "potential energy landscape" is defined simply by setting the energy levels of the two states $x \in \{A, B\}$. The U^{store} energy levels are $E_A = E$ and $E_B = 0$ so that the equilibrium distribution over the two states is given by $\rho_0 = (\Pr(X_0 = A), \Pr(X_0 = B)) = (p_E, 1-p_E)$. Then, U^{comp} swaps the two energy levels so that $E_A = 0$ and $E_B = E$. Let τ be long enough that the system has time to equilibrate to U^{comp}, yielding $\rho_\tau = (1 - p_E, p_E)$. Using Eq. (26) reveals only three possible outcomes for $\Sigma(x_0, x_\tau)$:

$$\begin{aligned}\Sigma(A, A) &= \Sigma(B, B) \\ &= 0 \\ \Sigma(B, A) &= -\Sigma(A, B) \\ &= 2\beta E \ .\end{aligned}$$

Since the system has been given time to equilibrate, the state at time $t = 0$ is not correlated with the state at time $t = \tau$. And so, the probabilities of these different events can be readily calculated, yielding the complete distribution of entropy production:

$$\begin{aligned}\Pr(\Sigma(A, A)) &= \Pr(\Sigma(B, B)) \\ &= p_E(1 - p_E) \\ \Pr(\Sigma(A, B)) &= p_E^2 \\ \Pr(\Sigma(B, A)) &= (1 - p_E)^2 \ .\end{aligned}$$

For the two-level system, $p_E = e^{-\beta E}/(1 + e^{-\beta E})$. For any antisymmetric function $Q(\Sigma) = -Q(-\Sigma)$, we have:

$$\begin{aligned}\langle Q(\Sigma)\rangle(E) &= Q(2\beta E)((1 - p_E)^2 - p_E^2) \\ &= Q(2\beta E)(1 - 2p_E) \\ &= Q(2\beta E)\frac{1 - e^{-\beta E}}{1 + e^{-\beta E}} \\ &= Q(2\beta E)\tanh(\beta E/2) \ .\end{aligned}$$

The zero-entropy events do not appear directly in the first line since $Q(0) = 0$ for any function Q that is odd in Σ. We use this to directly calculate both the average entropy production:

$$\langle\Sigma\rangle(E) = 2\beta E \tanh(\beta E/2) \ , \tag{E1}$$

and the minimum variance charge for the distribution (through Eq. (16)):

$$\begin{aligned}\epsilon^2_{Q\min}(E) &= \frac{1}{\langle\tanh(\Sigma/2)\rangle} - 1 \\ &= \frac{1}{\tanh(\beta E)\tanh(\beta E/2)} \ .\end{aligned} \tag{E2}$$

We then use parameter E to find the effective bound that Eq. (11) sets for a given average entropy production in the discrete reset process.

2. Reset

The reset simulation used nondimensionalized overdamped Lanvegin dynamics:

$$dx = -\Omega\partial_x U(x, t)dt + \xi\sqrt{2}\, r(t)\sqrt{dt} \ .$$

Here, $r(t)$ is a memoryless Gaussian variable, and all parameters and variables have been scaled to be dimensionless by the scheme $q' = q \cdot q_c$. q' is a dimensional quantity with q_c a scaling factor and q the dimensionless variable. The dimensionless simulation parameters Ω and ξ are combinations of the scaling factors and the familiar dimensional Langevin parameters. For all overdamped simulations $\Omega = \xi = 1$. This represents a relationship between the system's physical parameters, but the exact relationship is not important for our purposes. Note also

that we choose our scaling factor for energies to be $k_{\mathrm{B}}T$ so that the potential energy is in thermal energy units.

The computational potential used for the reset is shown in Fig. 3 and was held for $t_1 = 2$ time units. The left well is turned into a ramp leading in the right one, and the right well's energy is lowered. This causes nearly all process realizations to fall into the right well; hence the operation name *reset*. As the wells narrow, the variance of different work values conditioned on being in the left or right at $t = 0$ shrink. However, this distribution can never be bimodal due to the necessary presence of 0 entropy production events. As such, we expect the minimum scaled variance of any charge from these simulations to follow the "discrete bound" derived in following section.

To demonstrate that this class of protocol obeys the bound, a suite of 1366 simulations was performed using a Monte Carlo Markov Chain (MCMC) inspired approach to find parameters for which $\epsilon^2_{Q\mathrm{min}}$, as estimated by Eq. (16), is minimized. On each algorithm iteration, a new value was chosen for 2 (chosen randomly, with replacement) of the 4 parameters L, ℓ, D_0, D_1 using a Gaussian distribution centered on its current value, checking to make sure that $\ell < L$ and $D_0 > D_1$. After performing the simulation and measuring $\epsilon^2_{Q\mathrm{min}}$, the proposed parameter change was accepted with certainty if the new $\epsilon^2_{Q\mathrm{min}}$ was less than the original and accepted with a probability $p \propto e^{-\Delta\epsilon^2_{Q\mathrm{min}}}$ if it was greater. To keep the algorithm from exploring an untenable range of parameter space, jumps for which the average entropy production did not satisfy $1.5 \leq \langle\beta\Sigma\rangle \leq 6$ were rejected.

The end result is that for the simulations in Fig. 2 the parameters were sampled from the following ranges, though not uniformly or independently: $L \in (.2, 1.2)$, $\ell \in (0, 1.1)$, $D_0 \in (1, 6.2)$ and $D_1 \in (.2, 3.6)$. Here, L, ℓ are in units of the nondimensional position and D_0, D_1 in units of $k_{\mathrm{B}}T$.

3. Swap

The swap simulations used nondimensionalized underdamped Langevin dynamics:

$$\begin{aligned} dx &= v dt \\ dv &= -\lambda v dt - \Theta\partial_x U(x,t) dt + \eta\sqrt{2\lambda}\, r(t)\sqrt{dt}\ , \end{aligned}$$

A similar scaling strategy as that described for reset leads to three dimensionless parameters: λ, Θ, and η. $\Theta = \eta = 1$ for all simulations. However, λ, which parameterizes the system's coupling to its thermal environment, was allowed to vary.

The computational potential for the swap is a harmonic potential with $k = m\pi^2$; see Fig. 3. If $\lambda = 0$, the system undergoes a harmonic oscillation with a period of 2 time units. Exactly halfway through the oscillation, the particles that were in the left (right) well of U^{store} should now be located where the right (left) well is. Thus, turning U^{store} back on at $t_1 = 1$ implements a "swap" operation between asymmetric wells. Due to the underdamped dynamics, this type of protocol also persists in the case of nonzero λ: the system undergoes the same oscillation approximately, with some amount of dissipation and stochasticity. The work cost to implement this protocol approaches a bimodal distribution, with particles starting in the left well costing an energy value near $D_0 - D_1$ and those starting in the right yielding an energy surplus near $D_1 - D_0$. This distribution is sharpened by narrower wells and lower values of λ.

Rather than minimizing $\epsilon^2_{Q\mathrm{min}}$, the goal of this simulation is to demonstrate that $\epsilon^2_{Q\mathrm{min}}$ faithfully captures all cases—from where $\epsilon^2_{\mathrm{TGGL}}$ is tight to where ϵ^2_{BS} is tight to where neither is a good approximation. The protocol described above generates the bimodal distribution that saturates $\epsilon^2_{\mathrm{TGGL}}$ under some cases, but can also produce entropy production distributions where the minimal scaled variance is well above ϵ^2_{BS}.

To showcase this variety, an MCMC approach was again used. On each iteration of algorithm, a new value was chosen for 3 (chosen randomly, with replacement) of the 5 parameters L, ℓ, D_0, D_1, and λ using a Gaussian distribution centered on its current value, checking to make sure that $\ell < L$, $D_0 > D_1$, and $\lambda > 0$. In this case, all jumps for which $\langle\Sigma\rangle$ fell between 2 and 5 were accepted. And, those that did not were accepted with a probability that exponentially decayed in $|\langle\Sigma\rangle - 3.5|$. Figure 2 plots a suite of 1193 simulations, that stem from 8 different starting points for $\lambda \in (0, .15)$, but all other parameters the same. As the algorithm evolved, all free parameters were allowed to shift with the result being that parameters were sampled from the following ranges: $L \in (.14, .68)$, $\ell \in (0, .39)$, $D_0 \in (1.2, 10.5)$ and $D_1 \in (.39, 3.6)$, and $\lambda \in (0, .2)$.

4. Simulation Details

Each dot in the simulation plot was calculated from an ensemble of $50,000$ trajectories sampled from the equilibrium distribution, using a Monte Carlo method. To reduce errors, the averages shown in Fig. 2 were calculated using only the positive entropy production events according to Eq. (9), which assumes a system that obeys the TSCC DFT. This numerical trick does not alter any of the qualitative results, but allows for plots in which the error bars are small enough to not be relevant given

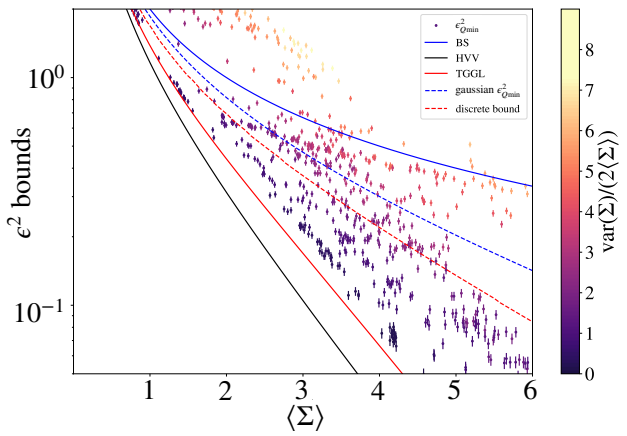

Figure 4. The same simulation data that in Fig. 2, but with 3σ error bars calculated from the full simulation, rather than only the well-sampled positive events.

the plot's scale. For example, Fig. 4 plots the same simulation data as that in Fig. 2, but with 3σ error bars calculated from the full simulation, rather than only the well-sampled positive events.

The Langevin simulations of the dimensionless equations of motion for both the underdamped and overdamped cases employed a fourth-order Runge-Kutta method for the deterministic portion and the Euler-Maruyama method for the stochastic portion of the integration with dt set to 5×10^{-5}. Python NumPy's Gaussian number generator was used to generate the memoryless Gaussian variable $r(t)$.

[1] Y. Dubi and M. Di Ventra. Colloquium: Heat flow and thermoelectricity in atomic and molecular junctions. *Rev. Mod. Phys.*, 83(1):131, 2011.

[2] V. Blickle and C. Bechinger. Realization of a micrometre-sized stochastic heat engine. *Nat. Phys.*, 8(2):143–146, 2012.

[3] I. A. Martínez, É. Roldán, L. Dinis, D. Petrov, J. M. R. Parrondo, and R. A. Rica. Brownian Carnot engine. *Nat. Phys.*, 12(1):67–70, 2015.

[4] J. Roßnagel, S.T. Dawkins, K.N. Tolazzi, O. Abah, E. Lutz, F. Schmidt-Kaler, and K. Singer. A single-atom heat engine. *Science*, 352(6283):325–329, 2016.

[5] M. Josefsson, A. Svilans, A.M. Burke, E.A. Hoffmann, S. Fahlvik, C. Thelander, M. Leijnse, and H. Linke. A quantum-dot heat engine operating close to the thermodynamic efficiency limits. *Nat. Nanotechnol.*, 13(10):920, 2018.

[6] G. Maslennikov, S. Ding, R. Hablützel, J. Gan, A. Roulet, S. Nimmrichter, J. Dai, V. Scarani, and D. Matsukevich. Quantum absorption refrigerator with trapped ions. *Nat. Commun.*, 10(1):1–8, 2019.

[7] J.P. S. Peterson, T.B. Batalhão, M. Herrera, A.M. Souza, R.S. Sarthour, I.S. Oliveira, and R.M. Serra. Experimental characterization of a spin quantum heat engine. *Phys. Rev. Lett.*, 123(24), 2019.

[8] D. Von Lindenfels, O. Gräb, C.T. Schmiegelow, V. Kaushal, J. Schulz, M.T. Mitchison, J. Goold, F. Schmidt-Kaler, and U.G. Poschinger. Spin heat engine coupled to a harmonic-oscillator flywheel. *Phys. Rev. Lett.*, 123(8):080602, 2019.

[9] G.T. Landi and M. Paternostro. Irreversible entropy production: From classical to quantum. *Rev. Mod. Phys.*, 93(3):035008, 2021.

[10] F.S. Gnesotto, F. Mura, J. Gladrow, and C.P. Broedersz. Broken detailed balance and non-equilibrium dynamics in living systems: a review. *Rep. Prog. Phys.*, 81(6):066601, 2018.

[11] T. Feldmann and R. Kosloff. The Quantum Four Stroke Heat Engine: Thermodynamic Observables in a Model with Intrinsic Friction. *Phys. Rev. E*, 68:016101, 2003.

[12] F. Plastina, A. Alecce, T.J.G. Apollaro, G. Falcone, G. Francica, F. Galve, N.L. Gullo, and R. Zambrini. Irreversible work and inner friction in quantum thermodynamic processes. *Phys. Rev. Lett.*, 113(26):260601, 2014.

[13] G. Francica, J. Goold, and F. Plastina. Role of coherence in the nonequilibrium thermodynamics of quantum systems. *Phys. Rev. E*, 99:042105, 2019.

[14] R. Dann and R. Kosloff. Quantum Signatures in the Quantum Carnot Cycle. *New J. Phys.*, 22:013055, 2020.

[15] R. Kubo. Brownian motion and nonequilibrium statistical mechanics. *Science*, 233(4761):330–334, 1986.

[16] L. Onsager. Reciprocal relations in irreversible processes. I. *Phys. Rev.*, 37(4):405, 1931.

[17] R. Kubo. The fluctuation-dissipation theorem. *Rep. Prog. Phys.*, 29(1):255, 1966.

[18] G. Gallavotti and E. G. D. Cohen. Dynamical ensembles in nonequilibrium statistical mechanics. *Phys. Rev. Lett.*, 74(14):2694–2697, 1995.

[19] C. Jarzynski. Nonequilibrium equality for free energy differences. *Phys. Rev. Lett.*, 78(14):2690, 1997.

[20] G.E. Crooks. Nonequilibrium Measurements of Free Energy Differences for Microscopically Reversible Markovian Systems. *J. Stat. Phys.*, 90:1481–1487, 1998.

[21] H. Tasaki. Jarzynski relations for quantum systems and some applications. *arXiv preprint cond-mat/0009244*, 2000.

[22] J. Kurchan. A quantum fluctuation theorem. *arXiv preprint cond-mat/0007360*, 2000.

[23] C. Jarzynski and D.K. Wójcik. Classical and quantum fluctuation theorems for heat exchange. *Phys. Rev. Lett.*, 92(23):230602, 2004.

[24] D. Andrieux, P. Gaspard, T. Monnai, and S. Tasaki. The

fluctuation theorem for currents in open quantum systems. *New J. Phys.*, 11:043014, 2009.

[25] K. Saito and Y. Utsumi. Symmetry in full counting statistics, fluctuation theorem, and relations among nonlinear transport coefficients in the presence of a magnetic field. *Phys. Rev. B: Condens. Matter*, 78(11):115429, 2008.

[26] M. Esposito, U Harbola, and S. Mukamel. Nonequilibrium fluctuations, fluctuation theorems, and counting statistics in quantum systems. *Rev. Mod. Phys.*, 81(4):1665, 2009.

[27] M. Campisi, P. Hänggi, and P. Talkner. Colloquium: Quantum fluctuation relations: Foundations and applications. *Rev. Mod. Phys.*, 83(3):771, 2011.

[28] C. Jarzynski. Equalities and inequalities: Irreversibility and the second law of thermodynamics at the nanoscale. *Annu. Rev. Condens. Matter Phys.*, 2(1):329–351, 2011.

[29] P. Hänggi and P. Talkner. The other QFT. *Nat. Phys.*, 11(2):108–110, 2015, 1311.0275.

[30] A.C. Barato and U. Seifert. Thermodynamic Uncertainty Relation for Biomolecular Processes. *Phys. Rev. Lett.*, 114(15):158101, 2015.

[31] T.R. Gingrich, J.M. Horowitz, N. Perunov, and J.L. England. Dissipation bounds all steady-state current fluctuations. *Phys. Rev. Lett.*, 116(12):120601, 2016.

[32] P. Pietzonka, F. Ritort, and U. Seifert. Finite-time generalization of the thermodynamic uncertainty relation. *Phys. Rev. E*, 96(1):012101, 2017, 1702.07699.

[33] A. Dechant. Multidimensional thermodynamic uncertainty relations. *J. Phys. A: Math. Gen.*, 52:035001, 2018, 1809.10414.

[34] J.M. Horowitz and T.R. Gingrich. Proof of the finite-time thermodynamic uncertainty relation for steady-state currents. *Phys. Rev. E*, 96(2):020103, 2017.

[35] A.C. Barato, R. Chetrite, A. Faggionato, and D. Gabrielli. Bounds on current fluctuations in periodically driven systems. *New J. Phys.*, 20(10):103023, 2018.

[36] V. Holubec and A. Ryabov. Cycling tames power fluctuations near optimum efficiency. *Phys. Rev. Lett.*, 121(12):120601, 2018.

[37] K. Proesmans and C. Van den Broeck. Discrete-time thermodynamic uncertainty relation. *Europhys. Lett.*, 119(2):20001, 2017.

[38] T. Van Vu and Y. Hasegawa. Thermodynamic uncertainty relations under arbitrary control protocols. *Phys. Rev. Res.*, 2(1):013060, 2020.

[39] H.J.D. Miller, M.H. Mohammady, M. Perarnau-Llobet, and G. Guarnieri. Thermodynamic uncertainty relation in slowly driven quantum heat engines. *Phys. Rev. Lett.*, 126(21):210603, 2021.

[40] H.J.D. Miller, M.H. Mohammady, M. Perarnau-Llobet, and G. Guarnieri. Joint statistics of work and entropy production along quantum trajectories. *Phys. Rev. E*, 103(5):052138, 2021.

[41] G. Falasco, M. Esposito, and J.C. Delvenne. Unifying thermodynamic uncertainty relations. *New J. Phys.*, 22(5):053046, 2020.

[42] Y. Hasegawa. Quantum thermodynamic uncertainty relation for continuous measurement. *Phys. Rev. Lett.*, 125(5):050601, 2020.

[43] Y. Hasegawa. Thermodynamic uncertainty relation for general open quantum systems. *Phys. Rev. Lett.*, 126(1):010602, 2021.

[44] T. Van Vu and K. Saito. Thermodynamics of precision in Markovian open quantum dynamics. *Phys. Rev. Lett.*, 128(14):140602, 2022.

[45] Y. Hasegawa. Unifying speed limit, thermodynamic uncertainty relation and Heisenberg principle via bulk-boundary correspondence. *Nat. Commun.*, 14(1), 2023.

[46] T. Van Vu and K. Saito. Thermodynamic unification of optimal transport: Thermodynamic uncertainty relation, minimum dissipation, and thermodynamic speed limits. *Phys. Rev. X*, 13(1), 2023.

[47] A. Dechant and S.I. Sasa. Fluctuation–response inequality out of equilibrium. *Proc. Natl. Acad. Sci. U.S.A.*, 117(12):6430–6436, 2020.

[48] K. MacIeszczak, K. Brandner, and J.P. Garrahan. Unified thermodynamic uncertainty relations in linear response. *Phys. Rev. Lett.*, 121:130601, 2018.

[49] G. Guarnieri, G.T. Landi, S.R. Clark, and J. Goold. Thermodynamics of precision in quantum nonequilibrium steady states. *Phys. Rev. Res.*, 1(3):033021, 2019.

[50] B.K. Agarwalla and D Segal. Assessing the validity of the thermodynamic uncertainty relation in quantum systems. *Phys. Rev. B*, 98(15):155438, 2018.

[51] S. Saryal, O. Sadekar, and B.K. Agarwalla. Thermodynamic uncertainty relation for energy transport in a transient regime: A model study. *Phys. Rev. E*, 103(2):022141, 2021.

[52] J. Liu and D. Segal. Coherences and the thermodynamic uncertainty relation: Insights from quantum absorption refrigerators. *Phys. Rev. E*, 103(3):032138, 2021.

[53] D.S.P. Salazar. Thermodynamic skewness relation from detailed fluctuation theorem. *arXiv preprint arXiv:2208.11206*, 2022.

[54] H.J.D. Miller, G. Guarnieri, M.T. Mitchison, and J. Goold. Quantum fluctuations hinder finite-time information erasure near the Landauer limit. *Phys. Rev. Lett.*, 125(16):160602, 2020.

[55] C. Jarzynski. Hamiltonian derivation of a detailed fluctuation theorem. *J. Stat. Phys.*, 98(1):77–102, 2000.

[56] G.E. Crooks. Entropy production fluctuation theorem and the nonequilibrium work relation for free energy differences. *Phys. Rev. E*, 60(3), 1999.

[57] Y. Hasegawa and T. Van Vu. Fluctuation theorem uncertainty relation. *Phys. Rev. Lett.*, 123(110602), 2019.

[58] D.J. Evans and D.J. Searles. The fluctuation theorem. *Adv. Phys.*, 51(7):1529–1585, 2002.

[59] P. M. Riechers, A. B. Boyd, G. W. Wimsatt, and J. P. Crutchfield. Balancing error and dissipation in computing. *Phys. Rev. Res.*, 2(3):033524, 2020.

[60] A.M. Timpanaro, G. Guarnieri, J. Goold, and G.T. Landi. Thermodynamic uncertainty relations from exchange fluctuation theorems. *Phys. Rev. Lett.*, 123(090604), 2019.

[61] A.C. Barato and U. Seifert. Thermodynamic uncertainty

relation for biomolecular processes. *Phys. Rev. Lett.*, 114(148101), 2015.

[62] J.M. Horowitz and T.R. Gingrich. Proof of the finite-time thermodynamic uncertainty relation for steady-state currents. *Phys. Rev. E*, 96(020103), 2017.

[63] Upendra Harbola, Massimiliano Esposito, and Shaul Mukamel. Statistics and fluctuation theorem for boson and fermion transport through mesoscopic junctions. *Phys. Rev. B*, 76:085408, 2007.

[64] D.M. Busiello and S. Pigolotti. Hyperaccurate currents in stochastic thermodynamics. *Phys. Rev. E*, 100(6):060102, 2019.

[65] M. Timpanaro, G. Guarnieri, G.T. Landi, et al. Hyperaccurate thermoelectric currents. *arXiv preprint arXiv:2108.05325*, 2021.

[66] T. Van Vu, V.T. Vo, and Y. Hasegawa. Entropy production estimation with optimal current. *Phys. Rev. E*, 101:042138, 2020.

[67] S. Otsubo, S. Ito, A. Dechant, and T. Sagawa. Estimating entropy production by machine learning of short-time fluctuating currents. *Phys. Rev. E*, 101:062106, 2020.

[68] S. Lee, D.K. Kim, J.M. Park, W.K. Kim, H. Park, and J.S Lee. Multidimensional entropic bound: Estimator of entropy production for Langevin dynamics with an arbitrary time-dependent protocol. *Phys. Rev. Res.*, 5:013194, 2023.

[69] D.K. Kim, Y. Bae, S. Lee, and H. Jeong. Learning entropy production via neural networks. *Phys. Rev. Lett.*, 125:140604, 2020.

[70] U. Seifert. Entropy production along a stochastic trajectory and an integral fluctuation theorem. *Phys. Rev. Lett.*, 95(4):040602, 2005.

[71] G.L. Jones. On the Markov chain central limit theorem. *Probab. Surv.*, 1(none):299 – 320, 2004.